Railway Slope Monitoring Based on Dual-Parameter FBG Sensor

Hongbin XU[1,2,4], Weiwei WANG[3], Feng LI[1,2,4*], Yanliang DU[1,2,4], Hongliang TU[5], and Chuanrui GUO[1,2,4]

[1]*College of Civil and Transportation Engineering, Shenzhen University, Shenzhen 518060, China*

[2]*National Key Laboratory of Green and Long-Life Road Engineering in Extreme Environment, Shenzhen University, Shenzhen 518060, China*

[3]*School of Civil Engineering, Shijiazhuang Tiedao University, Shijiazhuang 050043, China*

[4]*Institute of Urban Smart Transportation & Safety Maintenance, Shenzhen University, Shenzhen 518060, China*

[5]*State Key Laboratory of Geomechanics and Geotechnical Engineering, Institute of Rock and Soil Mechanics, Chinese Academy of Sciences, Wuhan 430071, China*

[*]Corresponding author: Feng LI E-mail: lf260986@semi.ac.cn

Abstract: A large number of slopes appear along the line during railway construction, which will pose a threat to railway safety operation. Slope monitoring plays an important role in ensuring the safety of railway operation. Aiming at the difficulties of sensor multiplexing, low accuracy, and large disturbance by trains, this paper proposes a railway slope monitoring method based on integrated fusion detection of inclination and vibration. Instability and failure characteristics of the K3 slope in Shuohuang Railway and dynamic characteristics under the excitation of the train load are analyzed by the finite element method (FEM) analysis. Based on the above analysis, a slope monitoring system is established utilizing the self-developed dual-parameter fiber Bragg grating (FBG) sensor. The monitoring data of the past four years show that the slope is in a relatively stable state at present. The monitoring data are consistent with the results of the FEM. The feasibility of the damage identification method based on inclination and vibration characteristics is verified, which provides a new method for railway slope monitoring.

Keywords: Fiber Bragg grating; railway slope; monitoring; inclination; vibration

Citation: Hongbin XU, Weiwei WANG, Feng LI, Yanliang DU, Hongliang TU, and Chuanrui GUO, "Railway Slope Monitoring Based on Dual-Parameter FBG Sensor," *Photonic Sensors*, 2025, 15(1), 250121.

1. Introduction

China's mountainous area accounts for about 2/3 of the country's total area. With the rapid development and construction of China's railways, a large number of natural and engineering slopes have appeared along the railways. Landslides, mudslides, and other geological disasters often occur in the bad weather, which has become the main hidden danger affecting safe operation of the transportation infrastructure. Reinforcement and monitoring are the main means of preventing and controlling disasters [1–3]. It is particularly necessary to monitor the high and steep slopes along the railway in real time in order to ensure a safe and smooth railway and improve the transportation efficiency. Much research

Received: 18 August 2023 / Revised: 4 January 2024
© The Author(s) 2024. This article is published with open access at Springerlink.com
DOI: 10.1007/s13320-024-0718-0
Article type: Regular

has focused on the slope slip monitoring technology. Among them, the inner deformation is the most intuitive and effective parameter to reflect the stability of the slope. Inner deformation monitoring can not only provide important information for the early warning of the slope instability but also help in predicting the sliding position and sliding volume of the slope.

At present, the most commonly used technology for slope-deep deformation monitoring is the borehole inclinometer technology based on an electrical inclinometer, which was put forward and developed by Wilson of Harvard University in 1952 [4]. The key point of this technology is to solve the accuracy problem of the sensor. With the development of the microelectronics technology represented by the micro-electro-mechanical system (MEMS) [5, 6], the slope deep deformation monitoring technology based on an electrical inclinometer is becoming more and more mature, and the monitoring method has also developed from the sliding monitoring technology [7] to the fixed monitoring technology [8], realizing the leap-forward development from traditional manual operation to automatic real-time monitoring. However, due to the limitation of the transmission distance of electrical signals, it is difficult to realize large-scale slope monitoring. At the same time, the number of sensors in each hole is limited due to the diameter of the signal line and sensor tube, resulting in low spatial resolution accuracy for inner deformation monitoring. In addition, the electrical displacement sensors [9] and time domain reflection technology [10, 11] are also used to monitor the inner deformation of the slope, but there are also problems, for example, poor electromagnetic interference resistance, large transmission loss, and short transmission distance.

The optical fiber sensing technology has the advantages of anti-electromagnetic interference [12−14], long-distance transmission [15], and easy reusing [16]. The optical fiber sensing technology has also been applied to deep deformation monitoring of slopes [17, 18], especially the fiber Bragg grating (FBG) sensing technology, which was once considered by some scholars as an alternative technology for slope monitoring and landslide early warning [19]. At present, much research is based on the FBG [20–22], Brillouin optical time domain analyzer (BOTDA) [23], Brillouin optical time domain reflectometer (BOTDR) [24], and optical time-domain reflectometry (OTDR) [25, 26] technology combining the fiber grating [27] or optical fiber [28] on the surface of the inclinometer tube, which produces strain along with the bending of the inclinometer tube, resulting in the change of the reflection spectrum and scattering spectrum in the optical fiber. Through the fiber grating demodulators and distributed demodulation technology, the deep deformation of the slope can be monitored. This method directly measures the surface strain of the inclinometer tube and obtains the deep deformation of the slope through integration, which has a large monitoring error, especially for high and steep slopes. The bottom of the inclinometer tube cannot be fixed, and the measurement results are easily distorted.

In addition, the train load vibration causes serious interference with the conventional railway slope monitoring system. With an increase in the traffic density and an increase in the vehicle speed and load, the interference of the train load vibration to the monitoring system becomes more and more serious. Through the study of the slope monitoring method based on the combination of the inclination angle and vibration (acceleration), not only the problem of train load vibration interfering with the monitoring system can be solved, but also the internal damage of the slope can be analyzed through the slope vibration response.

2. Shuohuang Railway

2.1 Slope status

Shuohuang Railway starts from Shenchi South

Station in Shenchi County, Shanxi Province, China in the west of China and ends at Huanghua Port Freight Yard in Cangzhou City, Hebei Province, China in the east of China. It was built on November 25th, 1997, and was opened to traffic on November 1st, 1999. The total length of the main line of the whole line is about 598 km. It is designed as a heavy-duty subgrade, a double-track electrified railway, and a national Class I trunk line. It is the second largest channel for transporting coal from the west to east in China and plays an important role in the national economic development. Shuohuang Railway passes through Taihang Mountain, Hengshan Mountain, Yunzhongshan Mountain, and other mountains, with complex topography, high mountains, and deep valleys, many high-filled embankments, and high-steep slopes, and there are potential safety hazards such as landslides or collapses. Therefore, it is of great significance to build a monitoring system for high-steep slopes along the railway to ensure the safe operation of the railway.

The Shenchi–Ningwu section of Shuohuang Railway belongs to a temperate continental monsoon climate, with long and cold winters, dry and windy springs, mild summers without intense heat, cool and rainy autumn, and obvious seasonal changes. The hillside in this area is gentle. The gully is developed, and there are a large number of artificial high-cut slopes along the line. Among them, 3 km of Shuohuang Railway is located in Longquan Town, Shenchi County, Shanxi Province (about 3 km away from Shenchi County), China, which is located in the loess hilly area. It belongs to the deep cutting slope. The slope is located on the side of the railway uplink line, in east-west direction, with a height of nearly 30 m, as shown in Fig. 1. Some areas of the slope are protected by concrete frame beams, the surface of the protected part is covered with the mortar rubble, and the surface of the unprotected part has sparse vegetation. The slope is new loess with the uniform soil quality and loose texture, which is easy to be eroded by running water. There are many bulges and cracks on the surface of the slope protection. The cracks are mostly distributed longitudinally along the line, and most of them are located in the middle of the slope protection and the contact part of the steps. The surface of the unprotected slope is seriously scoured by rain, and many scoured cracks and shallow slumps can be seen. Generally speaking, there are many diseases on the slope surface, and there are some hidden dangers that affect the safety of train operation.

Fig. 1 Shuohuang Railway in K3.

K3 of Shuohuang Railway is located at the end of the turn-back section of Shenchi South Station, where there are many railway lines, among which the main line of the ascending line is closest to the toe of the slope, and the outer rail is about 7.6 m away from the concrete retaining wall at the toe of the slope. In this chapter, the K3+200 section with severe erosion of unprotected parts is selected as the research object, which is a secondary slope with the new loess soil, and the section size is shown in Fig. 2.

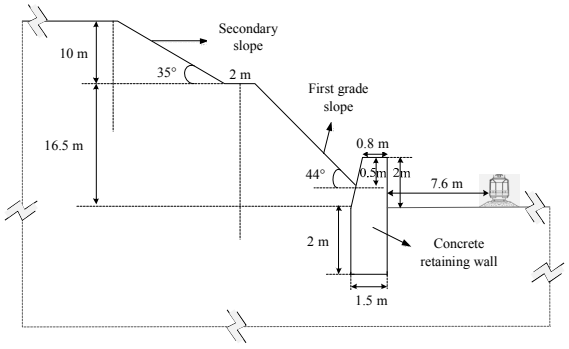

Fig. 2 Diagram of the slope at K3+200 of Shuohuang Railway.

2.2 Static characteristic analysis

The block discrete element program is used to simulate and analyze the whole process of the slope landslide. The mechanical parameters of the loess

and structural plane are listed in Table 1. The whole slope adopts the elastic-plastic constitutive model and Mohr-Coulomb yield criterion [29]. Under natural working conditions, the displacement constraints include: horizontal constraints are set on the left and right boundaries, vertical and horizontal constraints are set on the lower boundary, and the slope surface is a free boundary. Under the condition of a rainstorm, seepage boundary conditions are: the impermeable boundary is set on the left and right boundaries, the pore water pressure is set at 200 Pa on the slope (2 cm of surface water represents heavy rainfall), and the pore water pressure at the bottom boundary is set at 0 Pa.

Table 1 Material properties of the slope.

Geotechnical type	Attribute		Contact property		Cohesion (kPa)	Friction angle (°)	Tensile strength (MPa)
	Density (kg/m^3)	modulus of elasticity (MPa)	jk_n (GPa/m)	Jks (GPa/m)			
Loess	1410	23	9.5	9.5	16.8	25	0.25

Under the dead weight stress, the unbalanced force of the model is calculated, and the maximum unbalanced force of the system is less than 1×10^{-5} N after the model runs for 8000 steps. As shown in Fig. 3, the calculation converges, and the system is considered to be in equilibrium at this time, indicating that the loess slope is stable as a whole. By using the strength reduction method, the cohesion and friction angle of the material are reduced, and the deformation of the slope when it enters the limit equilibrium state is shown in Fig. 4 (the material properties of the slope are shown in Table 1). As shown in the figure, it can be seen that a penetrating slip plane is formed from the toe to the top of the slope. The reduction factor (slope safety factor) at this time is 1.32.

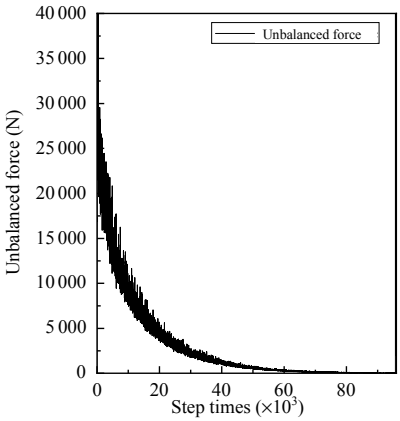

Fig. 3 Unbalanced force of the slope.

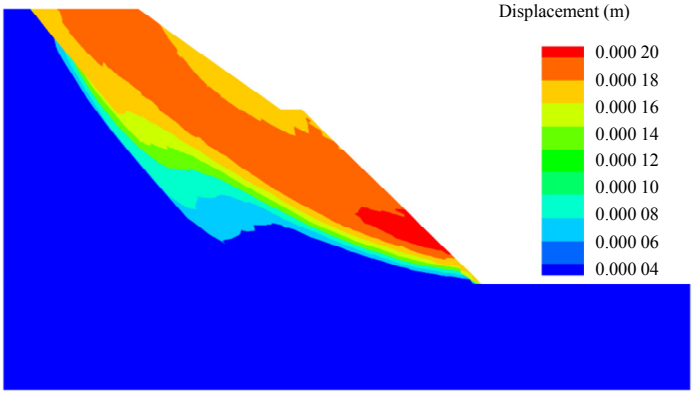

Fig. 4 Displacement of slope at the critical state of stability.

By applying the 200 Pa pore water pressure on the surface to simulate heavy rainfall, in the initial stress field, that is, after the self-weight calculation converges, the seepage calculation is started, and the lateral displacement changes at different depths from the tops of the first and second-grade slopes are shown in Fig. 5. It can be seen that, in the case of heavy rainfall, the first-grade slope is deformed first, and the deformation starts at the foot of the slope and eventually spreads to the whole slope surface. The initial deformation rate is slow. When the maximum deformation value of the first-grade slope reaches 0.6 m, the surface of the slope will suddenly collapse with a certain depth, and the collapse depth is about 6 m.

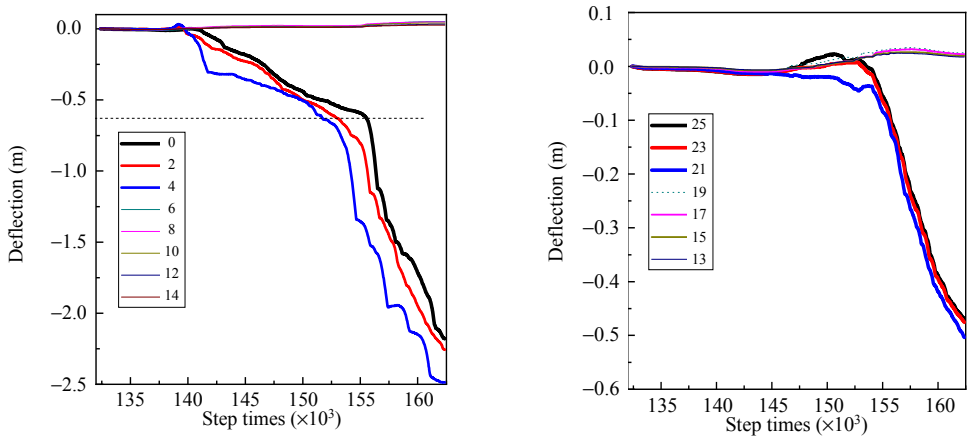

(a) (b)

Fig. 5 Displacement curve of the slope in different depths: (a) first grade slope platform and (b) top of the secondary slope.

2.3 Dynamic characteristic analysis

In this paper, the complete method is used for harmonic response analysis. A total of 250 kN excitation load is applied to 10 nodes within the range of 7.6 m–9.4 m from the concrete retaining wall (calculated according to the axle load of 25 tons of the C80 freight car), and the normal slope model and the slope model with 0.8 m thick soft layer (slip surface) are constructed, respectively. The free grid is used to divide the cells, and the cell size is controlled at 0.2 m. The models after cell division are shown in Fig. 6.

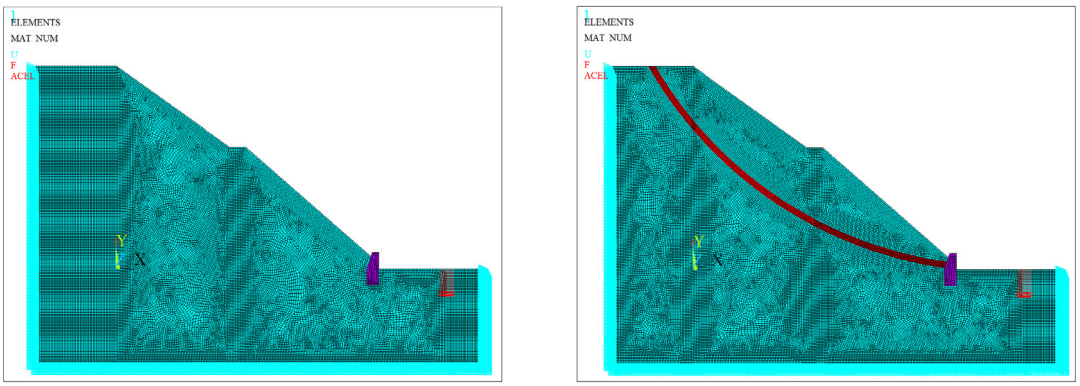

(a) (b)

Fig. 6 Harmonic analysis of the model: (a) normal slope model and (b) slope model with the weak layer (defect).

The LS-DYNA model is constructed by using plane162. The parameters, such as the model size and load, are the same as those in frequency domain analysis. The acceleration of different positions (nodes) in two slope structural models with or without weak layers under 20 Hz loading is shown in Fig. 7. As can be seen, on the whole, the closer it is to the surface, the greater the acceleration amplitude of the slope is. This is because in the case of micro-vibration, the soil is in the elastic deformation range of small strain, and the amplification of the soil layer can increase the vibration amplitude near the surface [30], especially the low-frequency component. The thicker the soil layer is, the closer it is to the surface, and the more obvious the effect is. The vibration intensity of the slope decreases obviously at the position of the weak layer and increases after passing through the weak layer, but it is less than that before passing through the weak layer. The acceleration cloud map

is shown in Fig. 8. As shown in Fig. 8, the acceleration distribution gradient is consistent with the propagation direction of the vibration wave, and the closer it is to the slope surface, the greater the acceleration peak value is. In the model with a weak layer, there is an obvious boundary at the weak layer of acceleration, which is caused by the obvious attenuation of acceleration when it passes through the weak layer.

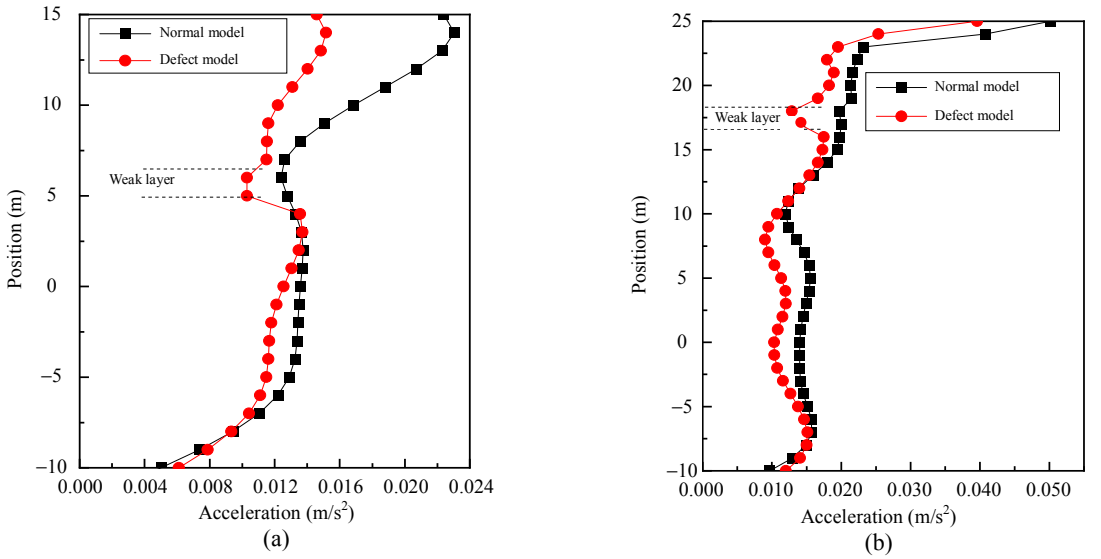

Fig. 7 Acceleration response of the slope at different positions: (a) acceleration response of the first grade slope and (b) secondary slope acceleration response.

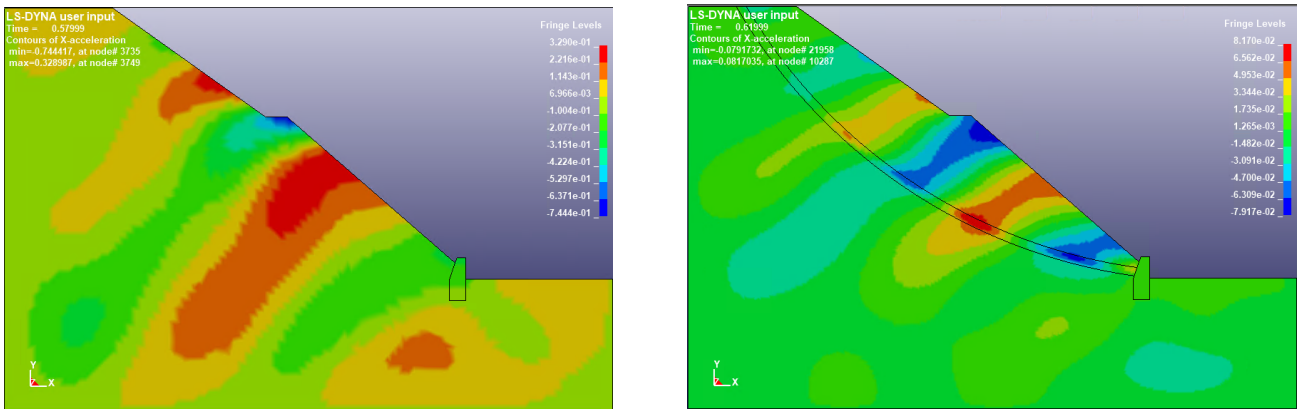

Fig. 8 Acceleration cloud map of the slope model: (a) normal model 0.58 s and (b) defect model 0.635 s.

3. Monitoring scheme and system construction

Combining with the above simulation results, a monitoring system is built in the middle of the unprotected area with the serious surface erosion. The monitoring scheme is shown in Fig. 9, including the in-situ dual-parameter FBG sensor [31], demodulator, optical cable, solar energy, 4G communication module, and monitoring center. The data are collected by the FBG demodulator based on the BaySpec module. The sensor and demodulator are connected by an optical cable. A wireless communication module is utilized for signal transmission between the demodulator and monitoring center. The on-site monitoring system is powered by the solar energy.

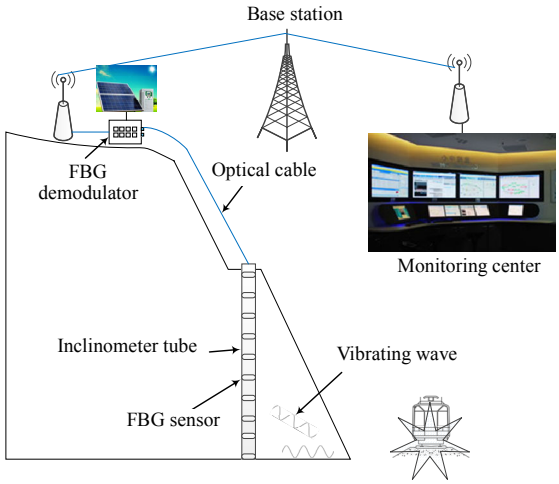

Fig. 9 Schematic diagram of the monitoring system.

The sensors are installed in a drilled hole, which is located at 1 m away from the front edge of the slope. Because of the hard soil, the rotary resistance of the drilling rig is very large. Water is used to reduce the resistance and prevent collapse during drilling.

In the process of drilling, when the borehole is drilled to about 7.5 m, gravel is encountered. As shown in Fig. 10, when the borehole is drilled to about 8 m, the slurry in the borehole leaks. The slurry is injected into the borehole no longer flowing back to the ground, so it can be inferred that there are unknown cracks in the slope. To ensure the depth of the borehole and minimize the influence of sediment precipitation in the mud on the depth of the borehole, it is necessary to clean the borehole before lifting the drill. Since the slurry leakage of the slope cannot flow back, to avoid the influence of over-grouting on the slope stability, the acrylonitrile butadiene styrene (ABS) inclinometer tube with a sealed bottom end should be lowered in time after drilling. When the ABS inclinometer tube encounters resistance during lowering, the orientation of the ABS inclinometer tube should be adjusted in time, so that two pairs of guide grooves distributed at 90 degrees in the ABS inclinometer tube are vertical and parallel to the slope, respectively. After adjusting the orientation, press the ABS inclinometer hard until the lowering length of the ABS inclinometer is close to the depth of the measuring hole.

(a) (b) (c)

Fig. 10 Gravel and installation of the ABS inclined pipe: (a) rhinestones carrying gravel, (b) gravel carried by the diamond, and (c) ABS inclinometer is lowered and installed.

To avoid the hole collapse, the gap between the ABS inclinometer tube and the hole wall of the measuring hole should be backfilled in time after the ABS inclinometer tube is lowered. To ensure that the slope deformation and vibration signals can be accurately transmitted to the ABS inclinometer, the

backfill material should have the same rigidity as the original soil. If the rigidity of the backfill material is too large or just too small, the deformation of the inclinometer will not match the deformation of the original soil, which will affect the monitoring accuracy. In the loess area, because the inclinometer hole is deep, it cannot be pounded, and the backfill state of the original soil is loose, so it is difficult to reach the original stiffness. The backfill mud in the loess is difficult to consolidate in a short time, and it is even more difficult to meet the original soil stiffness requirements. To ensure the backfill quality and prevent the backfill from being false, the backfill material should have certain fluidity, self-compaction, and high density. Therefore, gravel with a nominal diameter of 0.5 cm–1 cm is selected for backfilling, as shown in Fig. 11. To prevent the gravel from impacting the borehole wall and other factors from causing false backfilling, the backfilling speed should be slow, and the ABS inclinometer should be vibrated properly during the backfilling process to ensure the backfilling compactness. The sensor is installed by connecting the rod and guide wheel, as shown in Fig. 12. The sensor spacing is 2 m, and 9 FBG dual-parameter sensors are installed.

Under the influence of the scouring effect of the drilling rig circulating mud and hole collapse, the diameter of the borehole is usually larger than that of the drill bit, which leads to the actual amount of the backfill material far exceeding the calculated amount. Therefore, if the backfill amount is less than the calculated amount, it can be determined that the backfill is not dense. The drilling depth of the borehole is about 20 m, and the pipe running depth is 18.5 m. The theoretical backfill material is 0.14 m^3, and the actual material is nearly 1 m^3. This is not only the factor of the borehole diameter scouring and hole collapse, but also the gravel backfilling into the internal cracks of the slope through which the borehole passes.

Fig. 11 Backfilling of the borehole.

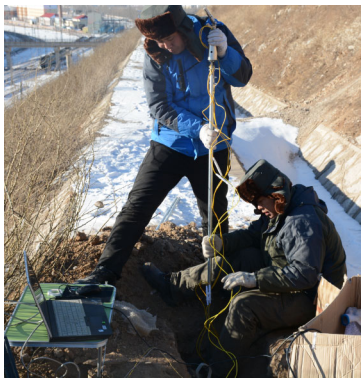

Fig. 12 Installation photo of the FBG sensors.

4. Monitoring results and analysis

4.1 Deep deformation analysis of the slope

The monitoring system was installed in November 2016, and the monitoring data of internal deformation of the slope are shown in Figs. 13 and 14. It can be seen that from November 2016 to August 2018, during the slope deformation stage, the internal displacement of the slope gradually increased, the maximum displacement was about 5.7 mm, and the average deformation rate was 3.25 mm/y. After August 2018, the slope basically turned into a stable period, and the internal displacement basically did not change. The reason for slope deformation may be that a large amount of slurry leaked during drilling and stored inside the slope, which led to a decrease in the loess strength inside the slope and even the collapse of loess, thus causing the internal deformation of the slope. With time, the moisture inside the soil gradually migrated and dissipated, the stability of the soil gradually recovered, and the internal deformation rate of the

slope gradually decreased until it reached a stable state. From Fig. 13, it can be seen that the deformation size of the slope turns at 11.5 m, and the deformation is larger at the position above 11.5 m. As far as the whole slope is concerned, there is no obvious slip surface on the slope.

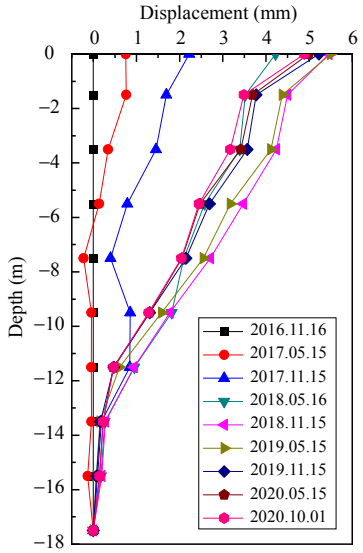

Fig. 13 Time-varying curve of the displacement in the primary slope.

From the above analysis, it can be seen that the slope is in a stable state as a whole, and the construction along the slope will have a certain impact on the slope stability. In the process of the slope construction (including sensor installation), the impact on the slope should be reduced, especially during the drilling operation before sensor installation, and the use of slurry should be minimized. Using miniaturized sensors and reducing the diameter of drilling holes can effectively reduce the difficulty of drilling holes and the influence of drilling holes on slopes.

It should be noted that the 13.5 m depth sensor of the slope failed in January 2017, and the 17.5 m depth sensor failed in May 2020. After the sensor fails, when calculating the deep deformation of the slope, the deformation at the position of the sensor is calculated according to the effective deformation before the sensor fails.

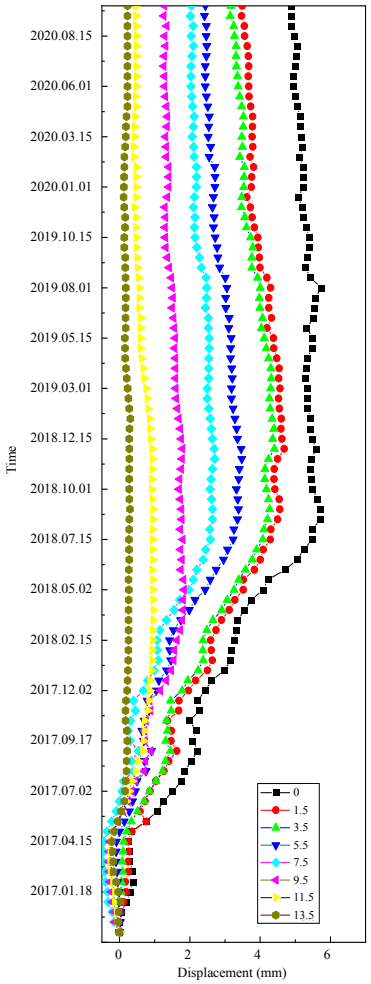

Fig. 14 Time-varying curve of the displacement in the primary slope.

4.2 Analysis of slope vibration characteristics

Under the excitation of the train, the strongest excitation frequency of each measuring point on the slope at different time points is shown in Fig. 15. As shown in the figure, the strongest frequency at the depth of 7.5 m decreases with time, with a variation range of 21.19 Hz–28.82 Hz and a frequency fluctuation range of about 7.63 Hz. The strongest frequency at the depth of 9.5 m on the slope increases with time, with a variation range of 9.42 Hz–21.08 Hz and a frequency fluctuation range of about 11.66 Hz. The strongest response frequency of other measuring points under the excitation of the train does not change obviously and is the strongest. Under the excitation of the train, the vibration amplitude of each measuring point on the slope is

shown in Fig. 16. As shown in the figure, the amplitude change is not obvious, which also shows that there is no obvious slip surface on the slope, which is mutually confirmed by the deformation data.

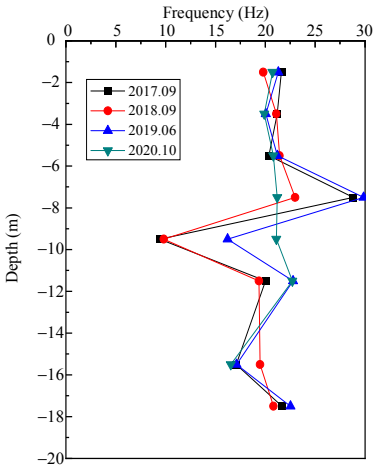

Fig. 15 Strongest frequency of each measuring point in the slope.

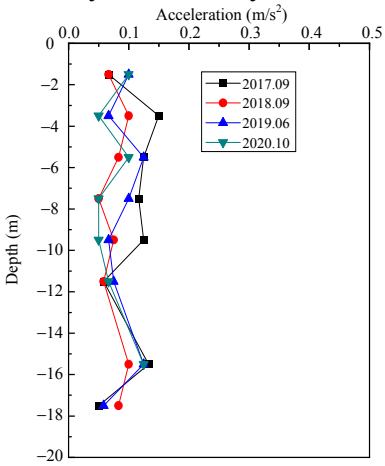

Fig. 16 Peak acceleration of each measuring point in the slope.

Typical spectrum characteristics of soil vibration are shown in Figs. 17–19. Under the excitation of the train along the line, the vibration of the slope with no defect position is shown in Fig. 17. As shown in the figure, the main vibration frequency is single and obvious, the signal-to-noise ratio is strong, and it is insensitive to the vehicle speed, vehicle type, and vehicle characteristics on the uplink and downlink lines.

At different times, the maximum response frequency of the train load excitation frequency changes greatly at the depths of 7.5 m and 9.5 m on the slope shown in Figs. 18 and 19. As shown in the

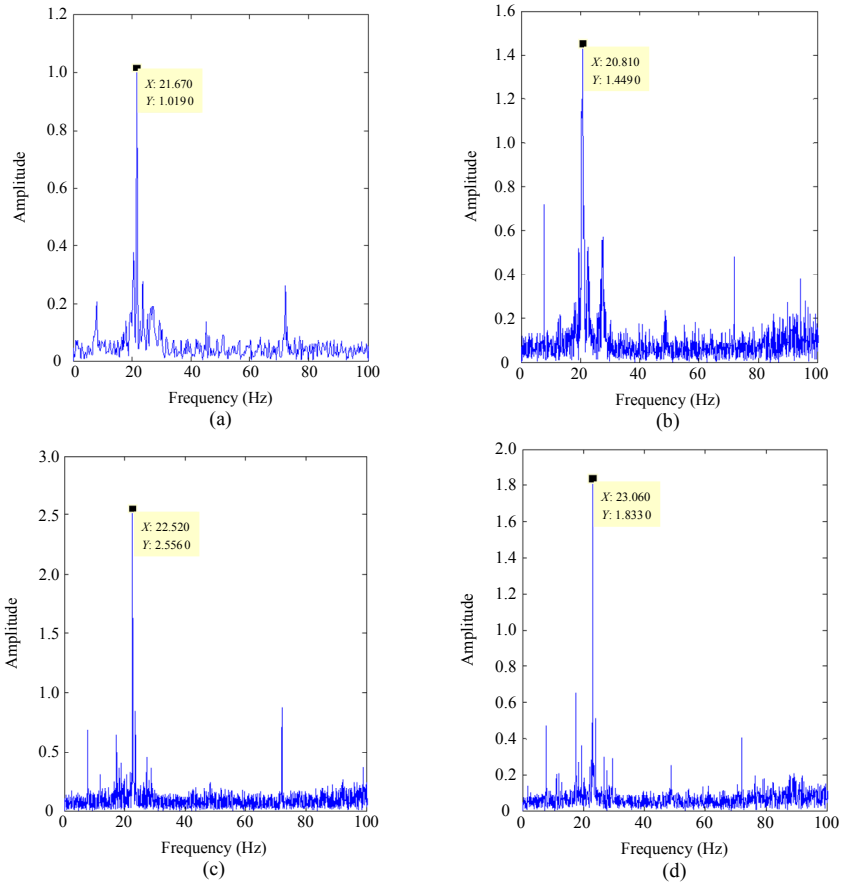

Fig. 17 Amplitude-frequency diagrams of slope in the depth of 17.5 m: (a) 2017.09, (b) 2018.09, (c) 2019.06, and (d) 2020.10.

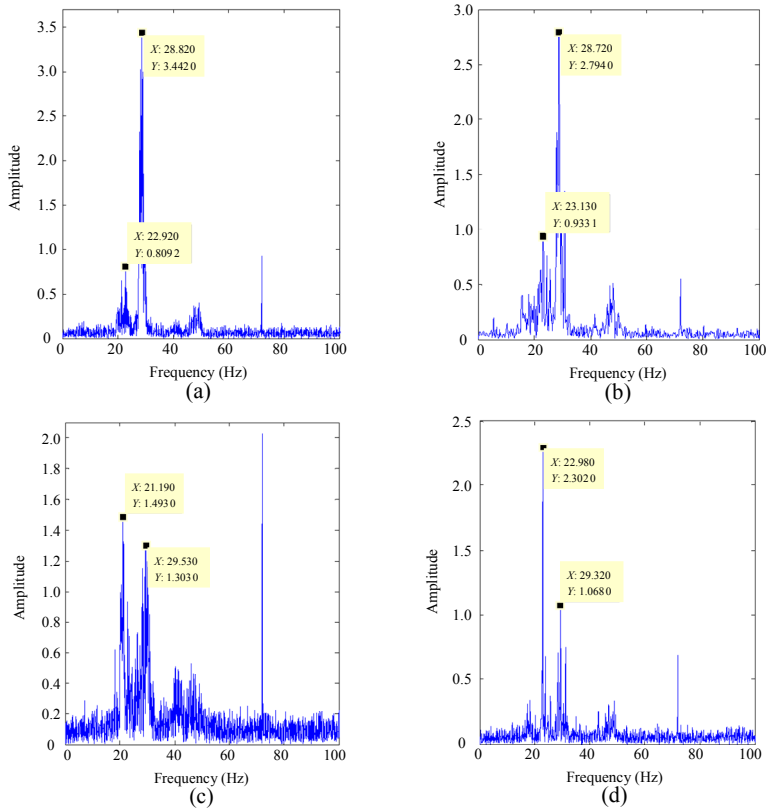

Fig. 18 Amplitude-frequency diagrams of slope in the depth of 7.5 m: (a) 2017.09, (b) 2018.09, (c) 2019.06, and (d) 2020.10.

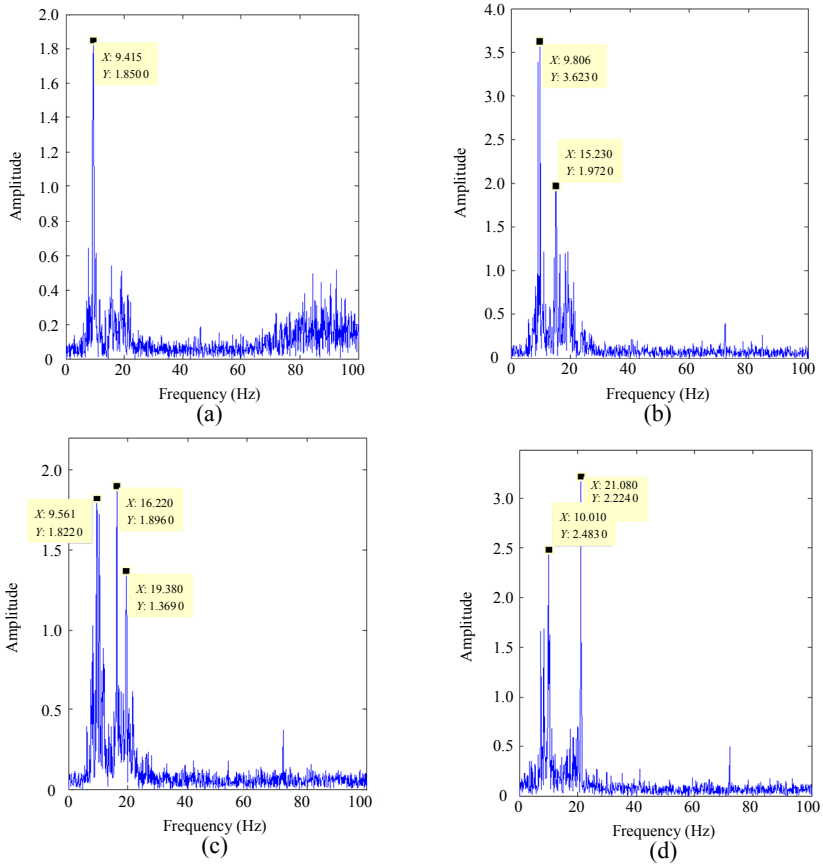

Fig. 19 Amplitude-frequency diagrams of the slope in the depth of 9.5 m: (a) 2017.09, (b) 2018.09, (c) 2019.06, and (d) 2020.10.

figures, there are more obvious response frequencies, and with time, its strongest response frequency is closer and closer to the strongest response frequency in other positions of the slope. Due to slurry leakage in the drilling process, it can be judged that there are unknown cracks, and a large amount of slurry is poured into the drilling process. After the inclinometer is installed and backfilled, it is surrounded by a mixture of the slurry and gravel, which leads to a change in the coupling state between the inclinometer and soil. The water in the mixture of mud and gravel diffuses with time, and the soil state gradually returns to and approaches the original state. This also verifies the feasibility of verifying the internal damage of the slope through the frequency change.

5. Conclusions

In this paper, a railway slope monitoring scheme utilizing FBG inclination and acceleration integrated sensor is proposed. Based on the results of finite element method (FEM), a slope monitoring system is constructed, and the monitoring data of the past four years are analyzed. The main conclusions are as follows:

(1) The FEM shows that the safety factor of the slope is 1.32. The inclination monitoring data show that the slope deformation curve has no obvious turning point, and the acceleration monitoring data show that the acceleration amplitude at different positions of the slope has no obvious change. The three results not only verify each other, but also show that the slope is in a stable state at present, and there is no obvious weak inter-layer and slip surface.

(2) The acceleration monitoring data show that the initial maximum response frequency of the slope at the positions of 7.5 m and 9.5 m is different from other positions. This difference decreases with the time, which is consistent with the occurrence of slurry leakage in the slope drilling process and the fact that the actual backfill gravel volume is greater than that of the theoretical calculation. These results verify the existence of unknown cracks and defects in the slope at the depth of 8 m.

(3) A slope monitoring method based on the inclination and vibration characteristics of the slope is proposed. The feasibility of this method is verified, which provides a new method for safety monitoring of the railway slope.

Acknowledgment

This work was supported in part by the National Key Research and Development Program of China (Grant No. 2021YFB2600800), National Natural Science Foundation of China (Grant No. 52378309), Shenzhen Science and Technology Program (Grant Nos. JCYJ20220818095608018 and KQTD20180412181337494), China Postdoctoral Science Foundation (Grant Nos. 2022M722188, 2022TQ0218, and 2022M722187), Natural Science Foundation of Hebei Province (Grant No. E2021210032), Visiting Researcher Fund Program of State Key Laboratory of Water Resources Engineering and Management (Grant No. 2022SGG05), and Tianjin Key Laboratory of Rail Transit Navigation Positioning and Spatio-temporal Big Data Technology (Grant No. TKL2024B10).

Declarations

Conflict of Interest The authors declare that they have no competing interests.

Permissions All the included figures, tables, or text passages that have already been published elsewhere have obtained the permission from the copyright owner(s) for both the print and online format.

Open Access This article is distributed under the terms of the Creative Commons Attribution 4.0 International License (http://creativecommons.org/licenses/by/4.0/), which permits unrestricted use, distribution, and reproduction in any medium, provided you give appropriate credit to the original author(s) and the source, provide a link to the Creative Commons license, and indicate if changes were made.

References

[1] B. Shi, H. H. Zhu, D. Zhang, and G. Cheng, “From in-situ rock-and-soil testing, exploration, monitoring

to sensing," *Journal of Engineering Geology*, 2022, 30(6): 1811–1818.

[2] Q. Xu, D. L. Peng, S. Zhang, X. Zhu, C. Y. He, X. Qi, *et al.*, "Successful implementations of a real-time and intelligent early warning system for loess landslides on the Heifangtai terrace, China," *Engineering Geology*, 2020, 278: 105817.

[3] Z. W. Wang, F. Li, and G. D. Mei, "OpenMP parallel finite-discrete element method for modeling excavation support with rockbolt and grouting," *Rock Mechanics and Rock Engineering*, 2024, 57: 3635–3657.

[4] T. D. Stark and H. Choi, "Slope inclinometers for landslides," *Landslides*, 2008, 5(3): 339–350.

[5] Y. Q. Shi, Y. F. Li, and L. F. Che, "Design of inclinometer based on MEMS accelerometer array," *Transducer and Microsystem Technologies*, 2020, 39(09): 66–68.

[6] Y. K. Cheung and H. Yu, "Electrochemical tilt sensors with symmetric concentric electrode pairs," *IEEE Sensors Journal*, 2021, 21(19): 21322–21329.

[7] G. W. Li, L. S. Hu, R. Wang, and D. Z. Chen, "Testing of slip inclinometer and error treatment methods," *Journal of Hohai University (Natural Sciences)*, 2013, 41(6): 511–517.

[8] H. Xu, F. Li, W. Zhao, S. Wang, Y. Du, and C. Bian, "A high precision fiber Bragg grating inclination sensor for slope monitoring," *Journal of Sensors*, 2019, 2019: 1354029.

[9] B. Q. Wu, W. D. Zhang, and Y. J. Yang, "Analysis on several commonly used side slope deep horizontal displacement monitoring technology," *Shanxi Architecture*, 2014, (19): 53–54.

[10] H. H. Tan and H. L. Fu, "Testing study of application of time domain reflectometry to highway slope monitoring," *Rock and Soil Mechanics*, 2010, 31(4): 1331–1336.

[11] D. F. Li, B. W. Zhang, G. Wang, K. B. Yang, L. M. Wang, and X. J. Xu, "Time domain reflectometry calculation model of landslides slippage," in *Proceedings of the Information Technology and Intelligent Transportation Systems*, Xi'an, China, 2017, 327–336.

[12] A. I. Azmi, A. S. Abdullah, M. M. Noor, M. H. Ibrahim, R. R. Ibrahim, T. Tan, *et al*., "Dynamic bending and rotation sensing based on high coherence interferometry in multicore fiber," *Optics & Laser Technology*, 2021, 135: 106716.

[13] J. J. Pan, L. Y. Wang, W. Hou, and H. Y. Lv, "Design and investigation of a high-sensitivity tilt sensor based on FBG," *Photonic Sensors*, 2023, 13(2), 230228.

[14] A. P. Zhang, S. Gao, G. Yan, and Y. Bai, "Advances in optical fiber Bragg grating sensor technologies," *Photonic Sensors*, 2012, 2(1): 1–13.

[15] Y. Cheng and Z. Shi, "Permanent deformation and temperature monitoring of subgrades using fiber Bragg grating sensing technology," *Journal of Sensors*, 2021, 2021: 8824058.

[16] D. F. Cao, H. H. Zhu, B. Wu, J. C. Wang, and S. K. Shukla, "Investigating temperature and moisture profiles of seasonally frozen soil under different land covers using actively heated fiber Bragg grating sensors," *Engineering Geology*, 2021, 290: 106197.

[17] X. L. Kuang, H. Zhang, L. P. Zhang, X. M. Yang, and M. H. Zhang, "Development and application of fibre grating inclinometer for monitoring the rock and soil slope deformation," *Highway*, 2015, 60(11): 171–176.

[18] J. Cui, D. S. Gunawardena, Z. Liu, Z. Zhao, and H. Y. Tam, "All-fiber two-dimensional inclinometer based on Bragg gratings inscribed in a seven-core multi-core fiber," *Journal of Lightwave Technology*, 2020, 38(8): 2516–2522.

[19] C. Y. Hong, Y. F. Zhang, M. X. Zhang, L. M. G. Leung, and L. Q. Liu, "Application of FBG sensors for geotechnical health monitoring, a review of sensor design, implementation methods and packaging techniques," *Sensors and Actuators A: Physical*, 2016, 244: 184–197.

[20] H. C. Li, C. T. Liu, and Y. B. Feng, "Application of FBG bending sensors in landslide forecasting and monitoring," *Journal of Optoelectronics Laser*, 2015, 26(2): 309–314.

[21] M. S. M. Sa'ad, H. Ahmad, M. A. Alias, M. K. A. Zaini, K. S. Lim, S. W. Harun, *et al*, "Surface-mounted tilt sensor using fiber Bragg grating technology for engineered slope monitoring with temperature compensation," *IEEE Sensors Journal*, 2023, 23(12), 12828–12837.

[22] J. Wang, W. Dong, W. Yu, C. Zhang, and H. Zhu, "Numerical and experimental investigation of slope deformation under stepped excavation equipped with fiber optic sensors," *Photonics*, 2023, 10(6): 692.

[23] X. L. Yi, H. M. Tang, Y. P. Wu, Y. Ge, X. Fan, and S. Zhang, "Application of the PPP-BOTDA distributed optical fiber sensor technology in the monitoring of the Baishuihe landslide," *Chinese Journal of Rock Mechanics and Engineering*, 2016, 35(S1): 3084–3091.

[24] Y. L. Liu, Y. Q. Shang, and Y. Yu, "Application of surface deformation monitoring of slope using BOTDR technology," *Journal of Jilin University* (*Earth Science Edition*), 2011, 41(3): 777–783.

[25] Z. Yu, H. Dai, Q. Zhang, M. Zhang, L. Liu, J. Zhang, *et al*., "High-resolution distributed strain sensing system for landslide monitoring," *Optik*, 2018, 158: 91–96.

[26] T. Kogure and Y. Okuda, "Monitoring the vertical distribution of rainfall-induced strain changes in a

landslide measured by distributed fiber optic sensing with Rayleigh backscattering," *Geophysical Research Letters*, 2018, 45(9): 4033–4040.

[27] F. Li, W. T. Zhang, F. Li, and Y. L. Du, "Fiber optic inclinometer for landslide monitoring," *Applied Mechanics & Materials*, 2012, 166–169: 2623–2626.

[28] W. J. Pang, Q. L. Deng, J. Xiong, and H. W. Wang, "Application study of optical fiber sensing technology to slope deformation monitoring based on BOTDA," *Safety and Environmental Engineering*, 2012, 19(6): 28–33.

[29] X. Q. Pi, L. Li, G. P. Tang, R. Zhang, and L. H. Zhao, "Stability analysis for soil slopes with weak interlayers using the finite element upper bound limit analysis," *Journal of Railway Science and Engineering*, 2019, 16(2): 351–358.

[30] Y. T. Ho, A. B. Huang, and J. T. Lee, "Development of a fibre Bragg grating sensored ground movement monitoring system," *Measurement Science and Technology*, 2006, 17(7): 1733–1740.

[31] H. Xu, F. Li, Y. Gao, and W. Wang, "Simultaneous measurement of tilt and acceleration based on FBG sensor," *IEEE Sensors Journal*, 2020, 20(24): 14857–14864.